

Dynamics of \bar{K} and multi- \bar{K} nuclei

D. Gazda,^{1,*} E. Friedman,^{2,†} A. Gal,^{2,‡} and J. Mares^{1,§}

¹*Nuclear Physics Institute, 25068 Řež, Czech Republic*

²*Racah Institute of Physics, The Hebrew University, Jerusalem 91904, Israel*

(Dated: February 1, 2008)

Abstract

We report on self-consistent calculations of single- K^- nuclear states and multi- \bar{K} nuclear states in ^{12}C , ^{16}O , ^{40}Ca and ^{208}Pb within the relativistic mean-field (RMF) approach. Gradient terms motivated by the p -wave resonance $\Sigma(1385)$ are found to play a secondary role for single- K^- nuclear systems where the mean-field concept is acceptable. Significant contributions from the $\bar{K}N \rightarrow \pi\Lambda$ conversion mode, and from the nonmesonic $\bar{K}NN \rightarrow YN$ conversion modes which are assumed to follow a ρ^2 density dependence, are evaluated for the deep binding-energy range of over 100 MeV where the decay channel $\bar{K}N \rightarrow \pi\Sigma$ is closed. Altogether we obtain K^- total decay widths of 50–100 MeV for binding energies exceeding 100 MeV in single- K^- nuclei. Multi- \bar{K} nuclear calculations indicate that the binding energy per \bar{K} meson saturates upon increasing the number of \bar{K} mesons embedded in the nuclear medium. The nuclear and \bar{K} densities increase only moderately and are close to saturation, with no indication of any kaon-condensation precursor.

PACS numbers: 13.75.Jz, 21.60.-n, 25.80.Nv, 36.10.Gv

Keywords: kaonic atoms; \bar{K} -nuclear bound states; density-dependent \bar{K} -nucleus interaction; \bar{K} -nuclear relativistic mean-field calculations; kaon condensation

*Electronic address: gazda@ujf.cas.cz

†Electronic address: elifried@vms.huji.ac.il

‡Electronic address: avragal@vms.huji.ac.il

§Electronic address: mares@ujf.cas.cz

I. INTRODUCTION

The subject of the present work is the study of \bar{K} meson interactions with the nuclear medium. It is closely related to one of the most important, so far unresolved problems in hadronic physics, of how hadron masses and interactions change within the nuclear medium. The in-medium properties of antikaons in dense nuclear matter have attracted considerable attention since the pioneering work of Kaplan and Nelson on the possibility of kaon condensation in dense matter [1, 2] and subsequent works offering related scenarios in nuclear matter [3, 4].

The existence of $\Lambda(1405)$, a $\bar{K}N$ quasi-bound state lying about 27 MeV below the K^-p threshold, suggests that the $\bar{K}N$ interaction is strongly attractive, as demonstrated first in a vector-meson exchange model due to Dalitz *et al.* [5]. This is consistent with low-energy $\bar{K}N$ scattering data [6] as well as with the measured level shift of the $1s$ state in the kaonic hydrogen atom [7, 8]. The $\Lambda(1405)$, as a K^-p quasi-bound state, was also corroborated in the Jülich meson exchange model [9], where the scalar σ and vector ω mesons act jointly to give strong attraction. Subsequent chiral SU(3) calculations showed that the $I = 0$ coupled-channel $\bar{K}N - \pi\Sigma$ interaction is sufficiently attractive to bind the $\Lambda(1405)$ [10, 11]. For an update on such calculations see Refs. [12, 13, 14].

The \bar{K} -nucleus interaction, too, is strongly attractive, as deduced from analyses of strong-interaction level shifts and widths in kaonic atoms [15, 16, 17, 18, 19, 20]. These fits to kaonic atom data are based on phenomenological density dependent optical potentials [15, 16, 17, 19, 20] or on a relativistic mean-field (RMF) approach [18], yielding strongly attractive K^- -nucleus potentials of depths 150–200 MeV. For an update see Ref. [21]. In contrast, coupled-channel calculations using $\bar{K}N$ interactions constrained by chiral models and fitted to the low-energy $\bar{K}N$ scattering and reaction data result in shallower \bar{K} -nucleus potentials of depth in the range of 100–150 MeV [22]. Imposing a self-consistency requirement on the evaluation of the in-medium \bar{K} -nucleus potential, yields much shallower potentials of depth about 50 MeV [23, 24, 25, 26]. Similar results are obtained when the Jülich meson-exchange model is used within a self-consistent coupled-channel calculation [27]. A depth of about 80 MeV is indicated by analyzing the enhanced near-threshold production of K^- mesons in proton-nucleus collisions, in recent experiments by the KaoS Collaboration at GSI [28] (and references cited therein to earlier nucleus-nucleus experiments).

The \bar{K} -nuclear interaction is also strongly absorptive, due dominantly to the one-nucleon absorption reactions $\bar{K}N \rightarrow \pi Y$ with approximately 100 MeV ($Y = \Sigma$) and 180 MeV ($Y = \Lambda$) energy release for the final hyperon Y . The strong absorptivity is confirmed by fits to kaonic-atom data [17].

Considerable interest in this field in recent years has focused on the question of possible existence of deeply bound \bar{K} -nuclear states, and whether such states are sufficiently narrow to allow unique experimental identification. Kishimoto [29], and Akaishi and Yamazaki [30, 31], suggested to look for \bar{K} -nuclear states bound by over 100 MeV, for which the dominant $\bar{K}N \rightarrow \pi\Sigma$ decay channel would become kinematically forbidden. Furthermore, it was suggested that multi- \bar{K} high-density nuclear clusters should also exist, providing perhaps a precursor stage to kaon condensation [32]. Several searches for \bar{K} deeply bound states have been subsequently made in KEK [33, 34, 35, 36], by the FINUDA collaboration in DAΦNE, Frascati [37] and at the AGS, Brookhaven [38]. However, the interpretation of the observed spectra is ambiguous, as demonstrated by an alternative explanation of the (allegedly K^-pp) peak observed in the back-to-back Λp invariant mass distribution of K^-_{stop} reactions on ${}^6,7\text{Li}$ and on ${}^{12}\text{C}$ [37] in terms of quasi-free K^-NN absorption and final-state interaction [39].

The theoretical calculations of \bar{K} -nuclear bound states may be divided into two classes: (i) few-body calculations using a single-channel G -matrix or AMD methodology [31, 40, 41, 42], and coupled-channel $\bar{K}NN - \pi\Sigma N$ Faddeev equations [43, 44] which agree with Refs. [31, 42] on K^-pp being bound, although differing widely on the binding energy and width calculated for this lightest possible system; (ii) dynamical RMF calculations [45, 46] which take into account the polarization of the nucleus owing to the strongly interacting \bar{K} meson, as well as the reduction of phase space available for the decay of the deeply bound \bar{K} meson. The calculations of Ref. [19] provide a lower limit of $\Gamma_{K^-} \simeq 50$ MeV on the width of nuclear bound states for K^- binding energy in the range $B_{K^-} \sim 100 - 200$ MeV.

The purpose of the present paper is twofold. In the first part we report on dynamical calculations of single- K^- nuclear states within the relativistic mean field (RMF) approach. This part of the work deals with three items:

- Effects due to the vector-meson ρ and ϕ mean fields which were not included in our previous calculations [45] are studied. The introduction of the ρ -meson mean field allows for a departure from $N = Z$ nuclear cores for \bar{K} -nuclear states, and the introduction

of the ϕ -meson mean field allows for studying multi-strange \bar{K} -nuclear states.

- The effect of p -wave gradient terms motivated by the $I = 1$ $\Sigma(1385)$ resonance is studied by extending the RMF coupled equations in the simplest form. Although the role of the $\bar{K}N$ p -wave interaction is marginal near threshold [47], it might become more important for deeply bound antikaons, owing to local variations in the nuclear densities induced by the antikaon [48].
- Following our previous work [45], we explore in more detail and rigor the absorptive part of the optical potential in the energy region where the dominant decay channel $\bar{K}N \rightarrow \pi\Sigma$ is closed. This is done by incorporating for the first time the $\bar{K}N \rightarrow \pi\Lambda$ channel, with threshold some 80 MeV below the $\pi\Sigma$ threshold, and by considering a ρ^2 density dependence for the two-nucleon absorption modes $\bar{K}NN \rightarrow YN$. The ρ^2 dependence is more appropriate for the description of the two-nucleon nature of these absorption modes.

In the second part of this work we explore within the RMF methodology deeply bound multi- \bar{K} nuclear states, in order to study the behavior of the nuclear medium under the influence of increasing strangeness. The issue here is whether or not the binding energy per \bar{K} meson of multi- \bar{K} nuclear states increases significantly upon adding a large number of \bar{K} mesons, so that \bar{K} mesons provide the physical degrees of freedom for self-bound strange hadronic systems. Kaon condensation in nuclear matter would occur beyond some threshold value of strangeness, if the binding energy per \bar{K} meson exceeds the combination $m_K + \mu_N - m_\Lambda \gtrsim 320$ MeV (in this paper we use $\hbar = c = 1$), where μ_N is the nucleon chemical potential. In such a case, Λ , Σ and Ξ hyperons would no longer combine macroscopically with nucleons to compose the more conventional kaon-free form of strange hadronic matter [49]. In neutron stars, the binding energy per \bar{K} meson necessary for the onset of kaon condensation is given by $m_K - \mu_{e-}$, where μ_{e-} is the electron chemical potential (generally accepted to assume values of $\mu_{e-} \lesssim 200$ MeV). The RMF approach was first applied to the study of kaon condensation in the mid 1990s, originally without considering a possible interplay with hyperons [50, 51] and then with hyperons included [52, 53]. This approach was also used in Ref. [54] to consider \bar{K}^0 condensation in addition to K^- condensation in neutron stars. Recent calculations offer a wide range of interesting precursor phenomena to kaon condensation in both hadronic and quark sectors (see Refs. [55, 56, 57, 58, 59] and

previous work cited therein). The present calculations may shed some light on the likelihood of a kaon-condensation scenario in nuclear matter.

The RMF methodology, including the extension to absorptive processes and p -wave gradient interaction terms, and to multi- \bar{K} nuclear states is discussed in Sec. II. Results of calculations for a representative set of nuclear cores across the periodic table are presented and discussed in Sec. III. Section IV summarizes the new results of the present work, along with conclusions and outlook.

II. MODEL

In the present work, \bar{K} -nuclear states are studied within the theoretical framework of the relativistic mean field (RMF) approach applied to a system of nucleons and one or more \bar{K} mesons. The interaction among hadrons is mediated by the exchange of scalar and vector meson fields. The standard RMF Lagrangian density \mathcal{L}_N describing the nucleonic sector is specified in Sec. III. The (anti)kaonic sector is incorporated by adding to \mathcal{L}_N the Lagrangian density \mathcal{L}_K :

$$\mathcal{L}_K = (\mathcal{D}_\mu K)^\dagger (\mathcal{D}^\mu K) - m_K^2 K^\dagger K + g_{\sigma K} m_K K^\dagger K \sigma, \quad (1)$$

with

$$K = \begin{pmatrix} K^+ \\ K^0 \end{pmatrix} \quad K^\dagger = \begin{pmatrix} K^- & \bar{K}^0 \end{pmatrix} \quad (2)$$

and the covariant derivative \mathcal{D}_μ given by:

$$\mathcal{D}_\mu \equiv \partial_\mu + i g_{\omega K} \omega_\mu + i g_{\rho K} \vec{\tau} \cdot \vec{\rho}_\mu + i g_{\phi K} \phi_\mu + i e \frac{1}{2} (1 + \tau_3) A_\mu. \quad (3)$$

This particular choice of interaction scheme leads to the coupling of the vector meson fields to conserved currents. The conserved (Noether) current associated with the kaonic field is obtained from the invariance of \mathcal{L}_K under global phase transformation. Using

$$K \rightarrow e^{i\lambda} K \quad \Rightarrow \quad \delta \mathcal{L}_K = 0 \quad \Rightarrow \quad \partial_\mu j_K^\mu = \partial_\mu \left[\frac{\delta \mathcal{L}_K}{\delta (\partial_\mu K)} \delta K + \delta K^\dagger \frac{\delta \mathcal{L}_K}{\delta (\partial_\mu K^\dagger)} \right] = 0, \quad (4)$$

one obtains a conserved vector current whose vacuum (represented by filled shells of nucleons and κ \bar{K} mesons) expectation value transforms to the expression for ρ_{K^-} given in Eq. (6) below. The standard variational principle yields equations of motion for all field operators. The meson field operators and source terms are then replaced by their expectation values,

according to the mean-field approximation. For simplicity, we limit discussion in this section to nuclear systems with K^- mesons. The generalization to nuclear systems with \bar{K}^0 mesons is straightforward.

Whereas the Dirac equation for nucleons is not explicitly affected by the addition of \mathcal{L}_K , the presence of K^- mesons induces additional source terms in the equations of motion for the meson (mean) fields:

$$\begin{aligned}
(-\nabla^2 + m_\sigma^2)\sigma_0 &= +g_{\sigma N}\rho_s + g_2\sigma_0^2 - g_3\sigma_0^3 + g_{\sigma K}m_K K^- K^+ \\
(-\nabla^2 + m_\omega^2)\omega_0 &= +g_{\omega N}\rho_v - g_{\omega K}\rho_{K^-} \\
(-\nabla^2 + m_\rho^2)\rho_0 &= +g_{\rho N}\rho_3 - g_{\rho K}\rho_{K^-} \\
(-\nabla^2 + m_\phi^2)\phi_0 &= -g_{\phi K}\rho_{K^-} \\
-\nabla^2 A_0 &= +e\rho_p - e\rho_{K^-},
\end{aligned} \tag{5}$$

with ρ_s , ρ_v and ρ_3 denoting the scalar, vector and isovector nuclear densities, respectively, and with ρ_p denoting the proton density. The K^- density ρ_{K^-} is given by:

$$\rho_{K^-} = 2(E_{K^-} + g_{\omega K}\omega_0 + g_{\rho K}\rho_0 + g_{\phi K}\phi_0 + eA_0)K^- K^+, \quad \int d^3x \rho_{K^-} = \kappa, \tag{6}$$

where $E_{K^-} = i\partial_t K^-$. The density ρ_{K^-} is normalized to the number of antikaons κ in a multi- K^- system.

The Klein–Gordon (KG) equation of motion for the K^- meson obtained from the RMF model acquires the form:

$$[-\nabla^2 - E_{K^-}^2 + m_K^2 + \text{Re } \Pi_{K^-}]K^- = 0, \tag{7}$$

where the K^- self-energy term is given by:

$$\begin{aligned}
\text{Re } \Pi_{K^-} &= -g_{\sigma K}m_K\sigma_0 - 2E_{K^-}(g_{\omega K}\omega_0 + g_{\rho K}\rho_0 + g_{\phi K}\phi_0 + eA_0) \\
&\quad - (g_{\omega K}\omega_0 + g_{\rho K}\rho_0 + g_{\phi K}\phi_0 + eA_0)^2.
\end{aligned} \tag{8}$$

This implies a K^- effective mass m_K^* of the form $m_K^{*2} = m_K^2 - g_{\sigma K}m_K\sigma_0$, in contrast to another possible choice [54] $m_K^* = m_K - g_{\sigma K}\sigma_0$. Qualitatively, our results are insensitive to this difference and the conclusions of the present study hold also for the other choice.

Assuming that all the K^- mesons occupy the same energy level, the total binding energy

of the combined κK^- -nuclear system $B(A, Z, \kappa K^-)$ has the form:

$$\begin{aligned}
B(A, Z, \kappa K^-) = & \sum_{i=1}^A B_i^{\text{sp}} + \kappa B_{K^-}^{\text{sp}} \\
& - \frac{1}{2} \int d^3x (-g_{\sigma N} \sigma_0 \rho_s + g_{\omega N} \omega_0 \rho_v + g_{\rho N} \rho_0 \rho_3 + e A_0 \rho_p) \\
& - \frac{1}{2} \int d^3x (-\frac{1}{3} g_2 \sigma_0^3 - \frac{1}{2} g_3 \sigma_0^4) \\
& + \frac{1}{2} \int d^3x [(g_{\omega K} \omega_0 + g_{\rho K} \rho_0 + g_{\phi K} \phi_0 + e A_0) \rho_{K^-} + g_{\sigma K} m_K \sigma_0 K^- K^+] ,
\end{aligned} \tag{9}$$

with $B_i^{\text{sp}} = m_N - E_i$ and $B_{K^-}^{\text{sp}} = m_K - E_{K^-}$, where E_i and E_{K^-} are the nucleon and K^- single particle energies, respectively. From this expression, it is evident that the K^- binding energy $B_{K^-} = B[A, Z, \kappa K^-] - B[A, Z, (\kappa - 1)K^-]$ contains, in addition to $B_{K^-}^{\text{sp}}$, mean field contributions representing part of the rearrangement energy of the nuclear core.

A. P-wave contributions

To study the role of p waves in the $\bar{K}N$ interaction, we have extended the K^- self energy Π_{K^-} by adding a phenomenological isoscalar p -wave potential:

$$\Pi_{K^-}^{(P)} = 4\pi \left(1 + \frac{E_{K^-}}{m_N} \right)^{-1} c_0 (\nabla \rho_v) \cdot \nabla , \tag{10}$$

where $c_0 = (c_p + c_n)/2 \approx 3c_p/2$ is an energy-dependent strength parameter dominated by the contribution of the $\Sigma(1385)$ p -wave resonance [60]. Calculations were done for K^- -nuclear states bound by about 100 MeV, corresponding roughly to $\sqrt{s_{\bar{K}N}} = 1330$ MeV, namely about 55 MeV below the $\Sigma(1385)$ resonance, where c_0 is positive (attractive) and nearly real:

$$c_0(1330 \text{ MeV}) = \frac{3}{2} c_p(1330 \text{ MeV}) = 0.186 \text{ fm}^3 , \tag{11}$$

in agreement with the plot of c_p in Fig. 2 of Ref. [42].

B. Absorptive contributions

Having dealt with the nuclear binding energy of K^- mesons, in the next step we consider \bar{K} absorption in the nuclear medium, in order to evaluate the K^- decay width Γ_{K^-} . In our model, this is done by allowing the self energy Π_{K^-} to become complex and replacing $E_{K^-} \rightarrow E_{K^-} - i\Gamma_{K^-}/2$. Since the imaginary part of the self energy is not addressed by

the traditional RMF approach, $\text{Im } \Pi_{K^-}$ was taken from optical model phenomenology. We follow Ref. [45] taking the optical potential imaginary-part depth from fits to K^- atomic data, while the nuclear density is treated as a dynamical quantity in these self-consistent calculations. Once the antikaon is embedded in the nuclear medium, the attractive $\bar{K}N$ interaction compresses the nuclear core, thus increasing the nuclear density which leads to an increased \bar{K} width. On the other hand, the phase space available for decay products is reduced due to the binding energy of the \bar{K} meson, particularly in the case of \bar{K} deeply bound states. To accomplish this reduction, suppression factors multiplying $\text{Im } \Pi_{K^-}$ were introduced, explicitly considering \bar{K} binding energy for the initial decaying state and assuming two-body final state kinematics.

We first consider absorption on a single nucleon, leading to the following pionic decay modes:

$$\bar{K}N \rightarrow \pi\Sigma, \pi\Lambda \quad (70\%, 10\%), \quad (12)$$

with thresholds about 100 MeV and 180 MeV, respectively, below the $\bar{K}N$ total mass. The numbers in parentheses give approximately the branching ratios known from bubble chamber and emulsion experiments [61]. The corresponding single-nucleon absorptive contribution to the optical potential is given in leading approximation by:

$$\text{Im } \Pi_{K^-}^{(1)} = (0.7f_{1\Sigma} + 0.1f_{1\Lambda}) W_0 \rho_v(r), \quad (13)$$

where W_0 is taken from kaonic atom fits and the phase-space suppression factors f_{1Y} ($Y = \Sigma, \Lambda$) are given by:

$$f_{1Y} = \frac{M_{01}^3}{M_1^3} \sqrt{\frac{[M_1^2 - (m_\pi + m_Y)^2][M_1^2 - (m_Y - m_\pi)^2]}{[M_{01}^2 - (m_\pi + m_Y)^2][M_{01}^2 - (m_Y - m_\pi)^2]}} \Theta(M_1 - m_\pi - m_Y), \quad (14)$$

with $M_{01} = m_K + m_N$ and $M_1 = M_{01} - B_{K^-}$.

Absorption on two nucleons leads to non-pionic decay modes

$$\bar{K}NN \rightarrow YN \quad (20\%), \quad (15)$$

with thresholds about $m_\pi \simeq 140$ MeV lower than the corresponding pionic decay mode thresholds. Since the non-pionic modes are heavily dominated by the ΣN final state, the ΛN channel was not considered in the present work and we focused attention primarily on a quadratic density dependence of the ΣN final-state contribution to the absorptive part of

the optical potential. A quadratic density dependence for two-nucleon absorption processes has been successfully used in studies of pionic atoms [17, 21]. The \bar{K} two-nucleon absorptive part of the optical potential is given by:

$$\text{Im } \Pi_{K^-}^{(2)} = 0.2 f_{2\Sigma} W_0 \rho_v^2(r)/\rho_0, \quad (16)$$

where the factor 0.2 represents the approximately 20% branching ratio for two-nucleon absorption from rest [61] and $\rho_0 \sim 0.16 \text{ fm}^{-3}$ is an A -dependent central nuclear density used for properly normalizing the two-nucleon absorption strength with respect to the one-nucleon absorption strength. The phase-space suppression factor $f_{2\Sigma}$ has the form:

$$f_{2\Sigma} = \frac{M_{02}^3}{M_2^3} \sqrt{\frac{[M_2^2 - (m_N + m_\Sigma)^2][M_2^2 - (m_\Sigma - m_N)^2]}{[M_{02}^2 - (m_N + m_\Sigma)^2][M_{02}^2 - (m_\Sigma - m_N)^2]}} \Theta(M_2 - m_\Sigma - m_N), \quad (17)$$

with $M_{02} = m_K + 2m_N$ and $M_2 = M_{02} - B_{K^-}$.

The set of coupled equations containing the Dirac equation for nucleons, the KG equations (5) and (7) for the meson mean fields and for antikaons, respectively, was solved self-consistently using an iterative procedure.

III. RESULTS AND DISCUSSION

Calculations of \bar{K} -nuclear states in ^{12}C , ^{16}O , ^{40}Ca , and ^{208}Pb were performed, using both the linear (HS) [62] and non-linear (NL-SH) [63] parameterizations of the nucleonic Lagrangian density \mathcal{L}_N . These RMF parameterizations give quite different estimates of nuclear properties. In particular, the non-linear models yield generally lower values of the nuclear incompressibility. Therefore, stronger polarization effects in these models owing to the presence of \bar{K} meson(s) are anticipated, in comparison with the linear models.

The (anti)kaon coupling constants to the meson fields were chosen as follows: The coupling constant $g_{\omega K}$ was given a reference value $g_{\omega K}^0 = (1/3)g_{\omega N}$ following the simple quark model. The reference value for $g_{\sigma K}$ was taken then from fits to kaonic atom data, which yielded $g_{\sigma K}^0 = 0.2 g_{\sigma N}$ for the linear and $g_{\sigma K}^0 = 0.233 g_{\sigma N}$ for the non-linear parameterizations of \mathcal{L}_N [18]. Finally, the coupling constants $g_{\rho K}$ and $g_{\phi K}$ were adopted from the $SU(3)$ relations: $\sqrt{2} g_{\phi K} = 2 g_{\rho K} = g_{\rho\pi} = 6.04$ [53].

The $SU(3)$ relation $2g_{\omega K} = g_{\rho\pi}$ was not imposed on $g_{\omega K}$ since its value was varied in the calculations, along with varying $g_{\sigma K}$, in order to scan over different values of \bar{K}

binding energies. Thus a particular way of varying these coupling constants away from their ‘reference’ values was used. Starting from $g_{iK} \equiv \alpha_i g_{iK}^0 = 0$ ($i = \sigma, \omega$), we first scaled up α_ω from the value required for the onset of binding all the way to $\alpha_\omega = 1$, corresponding to $g_{\omega K} = g_{\omega K}^0$. Then, for $\alpha_\omega = 1$, we scaled up α_σ from 0 to 1 corresponding to $g_{\sigma K} = g_{\sigma K}^0$, and finally we again scaled α_ω from 1 upwards until the binding energy value of $B_{\bar{K}} \simeq 200$ MeV was reached. Generally, similar results and conclusions are reached if different scanning procedures are applied. We comment below, for multi- \bar{K} nuclei, when this is no longer the case.

A. Single- K^- nuclei

In the first part of this work, single- K^- nuclear states were studied. We verified that the interaction generated by the ρ -meson mean field has a small effect on the K^- binding energy B_{K^-} and on the width Γ_{K^-} , for $B_{K^-} \lesssim 200$ MeV and for all the RMF parameterizations considered in the present work. This interaction acts repulsively on a K^- meson, producing a small decrease of B_{K^-} , less than 5 MeV in the case of ^{208}Pb where the most significant effect is anticipated due to the large excess of neutrons. The effect of the ρ meson field on the K^- decay width is even smaller, except in the region $60 \text{ MeV} \lesssim B_{K^-} \lesssim 100 \text{ MeV}$ where the phase-space suppression factor $f_{1\Sigma}$ varies rapidly and, hence, Γ_{K^-} increases by approximately 10 MeV.

Figure 1 shows the effect of the ρK^- coupling on the nucleon single-particle energies in ^{16}O . The left-hand spectrum shows the nucleon single-particle energies in the absence of K^- mesons, using the NL-SH model. The middle spectrum displays the rearrangement of these single-particle energies caused by a K^- meson bound by 100 MeV, with no ρK^- coupling. The most pronounced effect is observed for the $1s_{1/2}$ nucleon states, which become significantly more bound in the presence of a $1s$ K^- meson. The right-hand spectrum displays further modification of the nucleon single-particle energies due to the ρK^- coupling. It is seen that the isovector ρK^- interaction reverses the order of the $1s_{1/2}$ proton and neutron energy levels, determined in the absence of ρK^- coupling by the Coulomb interaction. This reversal is due to the ρK^- coupling acting against the Coulomb interaction.

The interaction generated by the ϕ -meson mean field reduces the K^- binding energy in systems with more than one K^- meson, as it mediates repulsive interaction exclusively

among strange particles. Generally, for the parameterizations and nuclei studied, the effect of the ϕ -meson repulsion increases with B_{K^-} , owing to the increased central K^- density. It amounts to several MeV for binding energies $B_{K^-} \lesssim 200$ MeV.

In the next step, considering the K^- decay modes discussed in the previous section, we calculated the corresponding widths of K^- -nuclear bound states. In particular, we considered the one-nucleon absorption mode $\bar{K}N \rightarrow \pi\Lambda$, in addition to the dominant $\bar{K}N \rightarrow \pi\Sigma$ mode studied in our recent work [45], and also both ρ and ρ^2 density dependencies of the two-nucleon absorption mode $\bar{K}NN \rightarrow \Sigma N$.

Figure 2 shows the calculated width Γ_{K^-} as a function of the binding energy B_{K^-} for the K^- $1s$ state in $^{12}_K\text{-C}$ (top) and in $^{40}_K\text{-Ca}$ (bottom), using the nonlinear model NL-SH. The effect of allowing the $\pi\Lambda$ decay mode (10%) to share alongside with $\pi\Sigma$ (70%) the one-nucleon absorption strength is shown by squares, compared to circles for the $\pi\Sigma$ mode alone (80%). In each of the two groups of curves shown (one for ρ and the other one for ρ^2 density dependence of the two-nucleon mode) the inclusion of the secondary $\pi\Lambda$ decay mode contributes approximately 20 MeV in $^{12}_K\text{-C}$ and 15 MeV in $^{40}_K\text{-Ca}$ to the width in the region of binding energies B_{K^-} between 100 and 160 MeV. As for the density dependence of the two-nucleon absorption mode, the widths calculated assuming ρ and ρ^2 density dependence are denoted by open and solid symbols, respectively. Assuming ρ^2 instead of ρ density dependence, it leads to increased widths of the $1s$ K^- -nuclear states, as demonstrated for $^{12}_K\text{-C}$ and $^{40}_K\text{-Ca}$ in Fig. 2, and for $^{16}_K\text{-O}$ in Fig. 3. The effect of the ρ^2 dependence of the $2N$ -absorption mode clearly grows with B_{K^-} as a consequence of the enhanced central nuclear density ρ_N . While for $B_{K^-} \lesssim 100$ MeV it is less than 10 MeV, for $B_{K^-} \gtrsim 150$ MeV it amounts to about 20 MeV in C and as much as about 30 MeV in Ca.

Figure 3 shows the widths Γ_{K^-} in $^{16}_K\text{-O}$ for the nonlinear model NL-SH (top) and in $^{208}_K\text{-Pb}$ for the linear model HS (bottom). As in the previous figure, switching on the $\pi\Lambda$ decay channel adds further conversion width to K^- -nuclear states. In the range $B_{K^-} \simeq 100 - 160$ MeV the width Γ_{K^-} increases by about 20 MeV. The $\pi\Lambda$ conversion mode disappears at $B_{K^-} \simeq 175$ MeV. The effect of the $\pi\Lambda$ absorption channel is almost uniform for both nonlinear (NL-SH in Fig. 2 and Fig. 3, top) and linear (HS in Fig. 3, bottom) parameterizations in all nuclei under consideration. On the other hand, the widths calculated assuming ρ^2 dependence for the two-nucleon absorption mode exhibit strong sensitivity to the type of RMF model applied and to the nucleus considered (via the nuclear

density ρ_N). In $^{208}_{K^-}\text{Pb}$, there is almost no difference between the widths Γ_{K^-} calculated using ρ or ρ^2 dependence. It was found that nonlinear parameterizations, represented here by NL-SH, produce larger increase of the width Γ_{K^-} owing to a ρ^2 density dependence of the $2N$ K^- absorption than linear models do, as could be anticipated from the considerably lower incompressibilities predicted by nonlinear models. It is to be noted that the particularly large widths Γ_{K^-} in $^{40}_{K^-}\text{Ca}$ for $B_{K^-} \gtrsim 150$ MeV are due to a more significant increase of the central nuclear density in $^{40}_{K^-}\text{Ca}$ than in $^{12}_{K^-}\text{C}$ within the NL-SH model, see Fig. 4.

Figure 4 demonstrates that the effect of nuclear compression, as evidenced by the increase of the nuclear density ρ_N upon increasing the binding energy B_{K^-} of the $1s$ state, is limited to relatively small radii, $r \lesssim 1.5$ fm. Whereas in as light a nucleus as C this region constitutes most of the nucleus, it is only a fraction of the nuclear volume in medium-weight nuclei such as Ca and in heavier nuclei (not shown in the figure).

We also studied another possible source of uncertainty for the calculated K^- decay width, namely the dependence on the branching ratios assumed for the various conversion modes. Figure 5 shows the K^- decay width Γ_{K^-} as a function of the K^- binding energy B_{K^-} in $^{16}_{K^-}\text{O}$ for the NL-SH model, assuming a ρ^2 dependence of the $2N$ -conversion mode. The branching ratios of the decay modes, $\bar{K}N \rightarrow \pi\Sigma : \bar{K}NN \rightarrow \Sigma N$, are varied from $0.7 : 0.3$ (circles) to $0.8 : 0.2$ (squares) and to $0.9 : 0.1$ (diamonds). The dotted curve represents the decay widths calculated when the $2N$ -absorption modes are neglected altogether. It is shown that varying the K^- absorption branching ratios by ± 0.1 away from the commonly used value $0.8 : 0.2$ alters the K^- decay width Γ_{K^-} by less than 10 MeV for binding energies $B_{K^-} \lesssim 90$ MeV. More remarkable is the effect in the region of $B_{K^-} \gtrsim 90$ MeV, where the dispersion reaches values of approximately 50 MeV. These results further point out to the delicacy of the estimates for the K^- decay widths in that region of binding energies. It is worth noting that the $0.8 : 0.2$ ‘canonical’ ratio is used here in a rather conservative way, implicitly assuming that it is effective for capture in the nuclear central-density region [see Eq. (16) for $\text{Im } \Pi_{K^-}^{(2)}$], whereas capture from rest in bubble-chamber and emulsion experiments [61] is likely to occur in lower-density regions. Therefore, the contribution to the K^- decay widths due to $\text{Im } \Pi_{K^-}^{(2)}$ could be larger than estimated by adopting the $0.8 : 0.2$ ‘canonical’ ratio. The ambiguities involved in evaluating the contribution of $\text{Im } \Pi_{K^-}^{(2)}$ have been recently discussed by Yamagata and Hirenzaki [64].

The last item studied for single- K^- nuclear states was the effect of a p -wave K^- -nucleus

TABLE I: p -wave interaction contributions to the K^- binding energy B_{K^-} , to the single-particle binding energy $B_{K^-}^{\text{sp}}$ and to the width Γ_{K^-} , for the $1s$ K^- -nuclear states in $^{12}_{K^-}\text{C}$ and in $^{40}_{K^-}\text{Ca}$, using the NL-SH parameterization. Results for s -wave interactions exclusively are denoted by S and results including the p -wave interaction Eqs. (10) and (11) are denoted by S+P.

	^{12}C			^{40}Ca		
	B_{K^-} (MeV)	$B_{K^-}^{\text{sp}}$ (MeV)	Γ_{K^-} (MeV)	B_{K^-} (MeV)	$B_{K^-}^{\text{sp}}$ (MeV)	Γ_{K^-} (MeV)
S	100.0	109.8	51.1	100.0	104.4	35.0
S+P	112.8	123.3	56.9	105.6	111.8	38.3

interaction $\Pi_{K^-}^{(P)}$ [Eq. (10)]. Table I demonstrates the effects of this interaction, with a strength parameter c_0 given by Eq. (11) for a nominal value of $B_{K^-} = 100$ MeV. Shown are the K^- binding energy B_{K^-} , the single-particle binding energy $B_{K^-}^{\text{sp}}$ and the decay width Γ_{K^-} , calculated for $1s$ K^- -nuclear states using the NL-SH parameterization. The results using the linear HS model are almost the same. The calculations excluding the p -wave K^- interaction are denoted by S, while those including the p -wave interaction are denoted by S+P. It is seen that the introduction of the p -wave interaction leads to an increase of the binding energy by approximately 13 MeV in $^{12}_{K^-}\text{C}$ and by approximately 6 MeV in $^{40}_{K^-}\text{Ca}$. The decay width is then enhanced by about 6 MeV for carbon and by about 3 MeV for calcium. This enhancement of the decay width is a consequence of the K^- binding energy dependence of Γ_{K^-} in the relevant region of B_{K^-} (see Fig. 2) and also of the moderate increase of the nuclear density distributions when compared to the case of purely s -wave interactions.

B. Multi- \bar{K} nuclei

In the second part of this work, we embedded several ($\kappa \geq 2$) antikaons in the nuclear medium and studied the nuclear response, as well as the energies and widths of bound states in such multi- \bar{K} nuclear systems. We studied nuclear systems containing only K^- mesons or only \bar{K}^0 mesons.

Figure 6 shows the calculated binding energies and widths of $1s$ K^- states in ^{16}O with two bound antikaons, using the NL-SH model, in comparison to similar calculations for a

single antikaon bound in ^{16}O . The K^- binding energy B_{K^-} of the second K^- in the double- K^- nucleus $^{16}_{2K^-}\text{O}$ is lower than the K^- binding energy in $^{16}_{1K^-}\text{O}$ for binding energies $B_{K^-} \lesssim 90$ MeV. Primarily, this is a consequence of the dominance of the mutual repulsion induced by the vector-meson mean fields between the two K^- mesons over the extra polarization of the nuclear core evoked by the presence of the second K^- meson. It is worth noting that this result is amplified by the larger width Γ_{K^-} in the case of two antikaons, which acts repulsively, and by setting $\alpha_\sigma = 0$, for the attractive interaction generated by the scalar mean field, at the low B_{K^-} region of the left-hand panels in the figure. (If the coupling of the K^- meson to *all* the vector-meson mean fields is switched off, so that B_{K^-} is generated solely via the scalar σ -meson mean field, and furthermore the imaginary potential is switched off, the binding energy B_{K^-} of the second K^- in $^{16}_{2K^-}\text{O}$ is *always* larger than B_{K^-} in $^{16}_{1K^-}\text{O}$.) This hierarchy is reversed at $B_{K^-} \simeq 90$ MeV when the K^- binding energy in $^{16}_{2K^-}\text{O}$ becomes larger than in $^{16}_{1K^-}\text{O}$, reflecting a strong polarization of the nuclear core (see Figs. 7 and 10). The enhancement of the binding energy B_{K^-} in the double K^- nucleus is then responsible for the crossings of the curves for the K^- decay widths Γ_{K^-} , at $B_{K^-} \simeq 90$ and 170 MeV, caused by the binding energy dependence of the suppression factors. Finally, the sharp decrease of the width Γ_{K^-} in $^{16}_{2K^-}\text{O}$, at $B_{K^-} \simeq 230$ MeV, is due to the disappearance of the $2N$ -absorption channel $\bar{K}NN \rightarrow \Sigma N$.

Figure 7 shows the average nuclear density $\bar{\rho}$ in ^{16}O and in ^{208}Pb with one and with two K^- mesons as a function of the K^- binding energy. Adding the second K^- to the nuclear system leads to further polarization of the nuclear core. The enhancement of the average nuclear density is quite pronounced in light nuclei (^{16}O) while in heavy nuclei (^{208}Pb) it is rather weak.

Figure 8 presents the 1s \bar{K} binding energy $B_{\bar{K}}$ in the multi- \bar{K} nuclei $^{16}\text{O} + \kappa\bar{K}$, where $\kappa\bar{K} = \kappa K^-$ or $\kappa\bar{K}^0$, as a function of the number of antikaons κ , calculated within the NL-SH RMF parameterization. The figure demonstrates that increasing the number of antikaons in the nuclear medium does not necessarily lead to a sizable increase of the binding energy $B_{\bar{K}}$. Just on the contrary, for relatively small values of $B_{\bar{K}}$ (the curve starting with 50 MeV for $\kappa = 1$ in the figure), $B_{\bar{K}}$ decreases as a function of κ . This is consistent with the trend shown in Fig. 6 for one and two K^- mesons. (Had we replaced the vector-meson mean-field couplings by an equivalent purely scalar-meson mean-field coupling to yield the same starting value of $B_{\bar{K}}$, setting also $\text{Im } \Pi_{\bar{K}} = 0$, $B_{\bar{K}}$ would rather increase as a function of κ .)

For the higher starting values for $B_{\bar{K}}$ in the figure, a moderate decrease of $B_{\bar{K}}$ as a function of κ occurs for $\kappa > 3$, indicating that the \bar{K} binding energies have reached saturation. We note that the difference between the K^- and \bar{K}^0 curves is relatively small, a few MeV at most, decreasing with κ owing to the increased role of the Coulomb repulsion among the K^- mesons.

Figure 9 shows the 1s \bar{K} binding energy in the multi- \bar{K} nuclei $^{208}\text{Pb} + \kappa\bar{K}$, where $\kappa\bar{K} = \kappa K^-$ or $\kappa\bar{K}^0$, calculated using the NL-SH model. It is found that the attractive Coulomb interaction of a K^- meson with the large number of protons ($Z = 82$ for ^{208}Pb) outweighs the repulsion due to the $\rho\bar{K}$ coupling, so that the lowest-energy configuration is provided by a purely K^- charge configuration. The K^- curves are displaced by about 15 MeV to higher values of binding energies than the respective \bar{K}^0 curves. Here and in the previous figure, the \bar{K}^0 couplings to the isoscalar-meson mean fields were taken identical to the corresponding K^- couplings, while differing in sign for the isovector ρ -meson mean field. Furthermore, $\text{Im } \Pi_{\bar{K}}$ was assumed to be the same for \bar{K}^0 mesons as for K^- mesons. For the lowest starting value of $B_{\bar{K}}$ in Fig. 9, as for ^{16}O in the previous figure, $B_{\bar{K}}$ decreases as a function of κ , although at a slower rate. For higher starting values of $B_{\bar{K}}$, a moderate increase of $B_{\bar{K}}(\kappa)$ is observed, which gradually slows down with increasing the number of antikaons κ . We checked that saturation of $B_{\bar{K}}(\kappa)$ is actually reached for a higher value of κ than shown in the figure ($\kappa \geq 10$).

The dependence of the nuclear density $\rho_N(r)$ and the K^- density $\rho_{K^-}(r)$ on the number of K^- mesons embedded in the nuclear medium is shown in Fig. 10 for ($^{16}\text{O} + \kappa K^-$) and in Fig. 11 for ($^{208}\text{Pb} + \kappa K^-$). Shown also for comparison, in dotted lines, are the density distributions ρ_N for $\kappa = 0$. The K^- couplings were chosen such that the $1K^-$ configuration was bound by 100 MeV. The density distributions behave quite regularly as a function of κ . In $^{16}\text{O} + \kappa K^-$, for $\kappa \geq 4$, the nuclear density distribution recovers the saddle it had without antikaons at $r \approx 0$. The increase of the nuclear density resulting from the 1s antikaons is limited to the vicinity of the nuclear center where the density ρ_{K^-} is substantial, much the same as for single- K^- nuclei (see Fig. 4) upon increasing B_{K^-} . The gradual increase of ρ_{K^-} as well as of ρ_N slows down with κ , leading to saturation as demonstrated for $\rho_N(0)$ in Figs. 10 and 11. The saturation is also apparent when the K^- densities ρ_{K^-} (normalized to κ) are shown as $\rho_{K^-}(0)/\kappa$ in Table II.

TABLE II: Values of $\rho_{K^-}(0)/\kappa$ (in fm^{-3}) as a function of the number of K^- mesons κ in ^{16}O and ^{208}Pb , using the NL-SH RMF parameterization. The K^- density ρ_{K^-} is normalized to κ . The K^- coupling constants for each core nucleus give rise to $B_{K^-} = 100$ MeV for a single K^- meson.

	κ	1	2	4	6	8	10
$\rho_{K^-}(0)/\kappa$	$^{16}\text{O} + \kappa K^-$	0.098	0.106	0.088	0.070		
$\rho_{K^-}(0)/\kappa$	$^{208}\text{Pb} + \kappa K^-$	0.009	0.010	0.013	0.014	0.015	0.013

IV. CONCLUSIONS

In the present work, we studied in detail the interplay between the underlying dynamical processes and the relevant kinematical conditions which determine the decay width of deeply bound \bar{K} -nuclear states in the nuclear medium. We performed fully self-consistent dynamical calculations of \bar{K} -nuclear states for nuclear systems with one and several \bar{K} mesons within the RMF approach.

We verified that the interaction of a $1s$ K^- meson with the ρ -meson mean field affects negligibly the K^- binding energy. Its main effect on the nucleon single particle energies is to partly cancel, and for the $1s$ nucleon level even reverse the $p - n$ Coulomb energy difference. For all nuclei and RMF parameterizations considered in the present work, the ρ -meson contribution slightly decreases the K^- binding energy B_{K^-} by less than about 5 MeV for $B_{K^-} \lesssim 200$ MeV. Similarly, the ϕ -meson contribution in systems with several K^- mesons reduces the K^- binding energy by a few MeV in this range of B_{K^-} values.

The calculations involving the p -wave interaction of the K^- meson with a nucleus indicate that the p -wave interaction plays a secondary role for deeply bound K^- -nuclear systems where the mean-field concept is acceptable. Although the p -wave interaction by itself is too weak to cause nuclear binding, its contribution in the lightest (carbon) nucleus considered in the present work amounts to more than 10 MeV and is certainly nonnegligible. Since the effect of the p -wave interaction appears to increase upon decreasing the atomic number, it could play a primary role in deeply and tightly bound few-body K^- systems.

We found that the implementation of the $\pi\Lambda$ decay channel in the single-nucleon absorption mode enhances the K^- conversion width for K^- binding energies $B_{K^-} \lesssim 170$ MeV. This enhancement is almost uniform for both linear and nonlinear parameterizations in all

nuclei considered. The most remarkable contribution occurs for K^- binding energies in the range $B_{K^-} \approx 100 - 160$ MeV where it reaches values of approximately 20 MeV. The assumption of a ρ^2 density dependence for the $2N$ -absorption mode adds further conversion width especially to the deeply bound K^- -nuclear states. The increase is particularly large for nonlinear parameterizations owing to the strong polarization effects affordable through the moderate value of nuclear incompressibility, as opposed to the highly unrealistic values in linear parameterizations. Altogether, the results of these comprehensive calculations suggest that K^- total decay widths for deeply bound K^- nuclear states ($B_{K^-} > 100$ MeV) are substantial, $\Gamma_{K^-} \sim 50 - 100$ MeV.

We also studied nuclear systems containing several antikaons. The nuclear and \bar{K} densities were found to behave quite regularly upon increasing the number of antikaons embedded in the nuclear medium. The calculations do not indicate any abrupt or substantial increase of the densities. The central nuclear densities in multi- K^- ^{16}O nuclei and in multi- K^- ^{208}Pb nuclei appear to saturate at about only 50% and 60%, respectively, higher values than the central nuclear densities in the corresponding systems with one antikaon. Furthermore, the \bar{K} binding energy saturates upon increasing the number of \bar{K} mesons embedded in the nuclear medium. The heavier the nucleus is, the more antikaons it takes to saturate the binding energies, but even for ^{208}Pb the number required does not exceed approximately 10. The saturated values of \bar{K} binding energies do not exceed the range of values 100–200 MeV considered normally as providing deep binding for one antikaon. This range of binding energies leaves antikaons in multi- \bar{K} nuclei comfortably above the range of energies where hyperons might be relevant. It is therefore unlikely that multi- \bar{K} nuclei may offer precursor phenomena in nuclear matter towards kaon condensation. This does not rule out that kaon condensation occurs in neutron stars where different constraints hold for the composition of matter. Although we presented results for one particular choice of RMF model, the NL-SH model [63], the use of other realistic mean-field models supports these conclusions.

Acknowledgments

One of us (AG) acknowledges and thanks Wolfram Weise for stimulating discussions, particularly on the \bar{K} -nuclear p -wave interaction. This work was supported in part by the

- [1] B.D. Kaplan, A.E. Nelson, Phys. Lett. B **175**, 57 (1986).
- [2] A.E. Nelson, B.D. Kaplan, Phys. Lett. B **192**, 193 (1987).
- [3] G.E. Brown, C.-H. Lee, M. Rho, V. Thorsson, Nucl. Phys. A **567**, 937 (1994).
- [4] C.-H. Lee, G.E. Brown, D.-P. Min, M. Rho, Nucl. Phys. A **585**, 401 (1995).
- [5] R.H. Dalitz, T.C. Wong, G. Rajasekaran, Phys. Rev. **153**, 1617 (1967).
- [6] A.D. Martin, Nucl. Phys. B **179**, 33 (1981).
- [7] M. Iwasaki *et al.*, Phys. Rev. Lett. **78**, 3067 (1997); T.M. Ito *et al.*, Phys. Rev. C **58**, 2366 (1998).
- [8] G. Beer *et al.*, Phys. Rev. Lett. **94**, 212302 (2005).
- [9] A. Müller-Groeling, K. Holinde, J. Speth, Nucl. Phys. A **513**, 557 (1990).
- [10] V. Koch, Phys. Lett. B **337**, 7 (1994).
- [11] N. Kaiser, P.B. Siegel, W. Weise, Nucl. Phys. A **594**, 325 (1995).
- [12] B. Borasoy, R. Nißler, W. Weise, Phys. Rev. Lett. **94**, 213401 (2005); *ibid.* **96**, 199201 (2006); Eur. Phys. J. A **25**, 79 (2005).
- [13] J.A. Oller, J. Prades, M. Verbeni, Phys. Rev. Lett. **95**, 172502 (2005); *ibid.* **96**, 199202 (2006); J.A. Oller, Eur. Phys. J. A **28**, 63 (2006); J.A. Oller, J. Prades, M. Verbeni, Eur. Phys. J. A **31**, 527 (2007).
- [14] B. Borasoy, U.-G. Meißner, R. Nißler, Phys. Rev. C **74**, 055201 (2006).
- [15] E. Friedman, A. Gal, C.J. Batty, Phys. Lett. B **308**, 6 (1993).
- [16] E. Friedman, A. Gal, C.J. Batty, Nucl. Phys. A **579**, 518 (1994).
- [17] C.J. Batty, E. Friedman, A. Gal, Phys. Rep. **287**, 385 (1997).
- [18] E. Friedman, A. Gal, J. Mareš, A. Cieplý, Phys. Rev. C **60**, 024314 (1999).
- [19] J. Mareš, E. Friedman, A. Gal, Nucl. Phys. A **770**, 84 (2006).
- [20] N. Barnea, E. Friedman, Phys. Rev. C **75**, 022202(R) (2007).
- [21] E. Friedman, A. Gal, Phys. Rep. **452**, 89 (2007).
- [22] T. Waas, N. Kaiser, W. Weise, Phys. Lett. B **365**, 12 (1996); *ibid.* **379**, 34 (1996).
- [23] J. Schaffner-Bielich, V. Koch, M. Effenberger, Nucl. Phys. A **669**, 153 (2000).
- [24] A. Ramos, E. Oset, Nucl. Phys. A **671**, 481 (2000).

- [25] A. Baca, C. García-Recio, J. Nieves, Nucl. Phys. A **673**, 335 (2000).
- [26] A. Cieplý, E. Friedman, A. Gal, J. Mareš, Nucl. Phys. A **696**, 173 (2001).
- [27] L. Tolos, A. Ramos, A. Polls, T.T.S. Kuo, Nucl. Phys. A **690**, 547 (2001).
- [28] W. Scheinast *et al.*, Phys. Rev. Lett. **96**, 072301 (2006).
- [29] T. Kishimoto, Phys. Rev. Lett. **83**, 4701 (1999).
- [30] Y. Akaishi, T. Yamazaki, in *Proc. III Int. Workshop on Physics and Detectors for DAΦNE*, edited by S. Bianconi *et al.*, Frascati Physics Series XVI (LNF, Frascati, 1999), p. 59.
- [31] Y. Akaishi, T. Yamazaki, Phys. Rev. C **65**, 044005 (2002).
- [32] T. Yamazaki, A. Doté, Y. Akaishi, Phys. Lett. B **587**, 167 (2004).
- [33] T. Suzuki *et al.*, Phys. Lett. B **597**, 263 (2004).
- [34] T. Suzuki *et al.*, Nucl. Phys. A **754**, 375c (2005).
- [35] M. Iwasaki *et al.*, arXiv:0706.0297 [nucl-ex].
- [36] T. Kishimoto *et al.*, Prog. Theor. Phys. **118**, 181 (2007).
- [37] M. Agnello *et al.*, Phys. Rev. Lett. **94**, 212303 (2005).
- [38] T. Kishimoto *et al.*, Nucl. Phys. A **754**, 383c (2005).
- [39] V.K. Magas, E. Oset, A. Ramos, H. Toki, Phys. Rev. C **74**, 025206 (2006).
- [40] T. Yamazaki, Y. Akaishi, Phys. Lett. B **535**, 70 (2002).
- [41] A. Doté, H. Horiuchi, Y. Akaishi, T. Yamazaki, Phys. Lett. B **590**, 51 (2004); Phys. Rev. C **70**, 044313 (2004); Y. Akaishi, A. Doté, T. Yamazaki, Phys. Lett. B **613**, 140 (2005).
- [42] A. Doté, W. Weise, arXiv:nucl-th/0701050.
- [43] N.V. Shevchenko, A. Gal, J. Mareš, Phys. Rev. Lett. **98**, 082301 (2007); Phys. Rev. C **76**, 044004 (2007).
- [44] Y. Ikeda, T. Sato, Phys. Rev. C **76**, 035203 (2007).
- [45] J. Mareš, E. Friedman, A. Gal, Phys. Lett. B **606**, 295 (2005); Nucl. Phys. A **770**, 84 (2006).
- [46] X.H. Zhong, G.X. Peng, L. Li, P.Z. Ning, Phys. Rev. C **74**, 034321 (2006).
- [47] C. García-Recio, J. Nieves, E. Oset, A. Ramos, Nucl. Phys. A **703**, 271 (2002).
- [48] S. Wycech, A.M. Green, arXiv:nucl-th/0501019.
- [49] J. Schaffner-Bielich, A. Gal, Phys. Rev. C **62**, 034311 (2000).
- [50] J. Schaffner, A. Gal, I.N. Mishustin, H. Stöcker, W. Greiner, Phys. Lett. B **334**, 268 (1994).
- [51] G.E. Brown, M. Rho, Nucl. Phys. A **596**, 503 (1996).
- [52] R. Knorren, M. Prakash, P.J. Ellis, Phys. Rev. C **52**, 3470 (1995).

- [53] J. Schaffner, I.N. Mishustin, Phys. Rev. C **53**, 1416 (1996).
- [54] S. Pal, D. Bandyopadhyay, W. Greiner, Nucl. Phys. A **674**, 553 (2000).
- [55] T. Maruyama, T. Muto, T. Tatsumi, K. Tsushima, A.W. Thomas, Nucl. Phys. A **760**, 319 (2005).
- [56] G.E. Brown, C.-H. Lee, H.-J. Park, M. Rho, Phys. Rev. Lett. **96**, 062303 (2006).
- [57] C.Y. Ryu, C.H. Hyun, S.W. Hong, B.T. Kim, Phys. Rev. C **75**, 055804 (2007).
- [58] Y. Kim, K. Kubodera, D.-P. Min, F. Myhrer, M. Rho, Nucl. Phys. A **792**, 249 (2007).
- [59] T. Muto, arXiv:nucl-th/0702027.
- [60] W. Weise, arXiv:nucl-th/0701035.
- [61] C. Vander Velde-Wilquet, J. Sacton, J.H. Wickens, D.N. Tovee, D.H. Davis, Nuovo Cimento A **39**, 538 (1977).
- [62] C.J. Horowitz, B.D. Serot, Nucl. Phys. A **368**, 503 (1981).
- [63] M.M. Sharma, M.A. Nagarajan, P. Ring, Phys. Lett. B **312**, 377 (1993).
- [64] J. Yamagata, S. Hirenzaki, Eur. Phys. J. A **31**, 255 (2007).

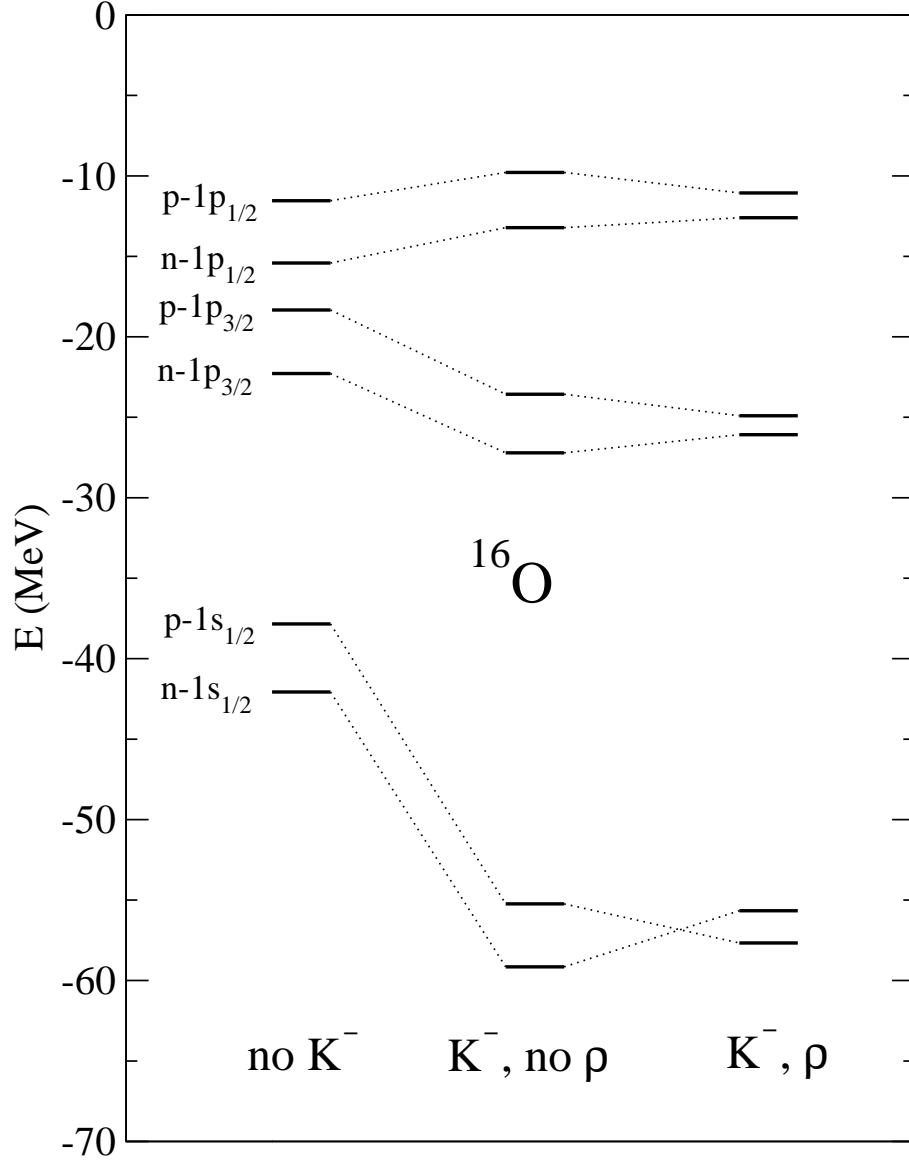


FIG. 1: Nucleon single-particle energies with respect to the nucleon mass in ^{16}O (left spectrum) and in $^{16}_{K^-}\text{O}$ (middle and right spectra) for $B_{K^-} = 100$ MeV, with and without coupling the K^- meson to the ρ -meson mean field, using the NL-SH RMF model.

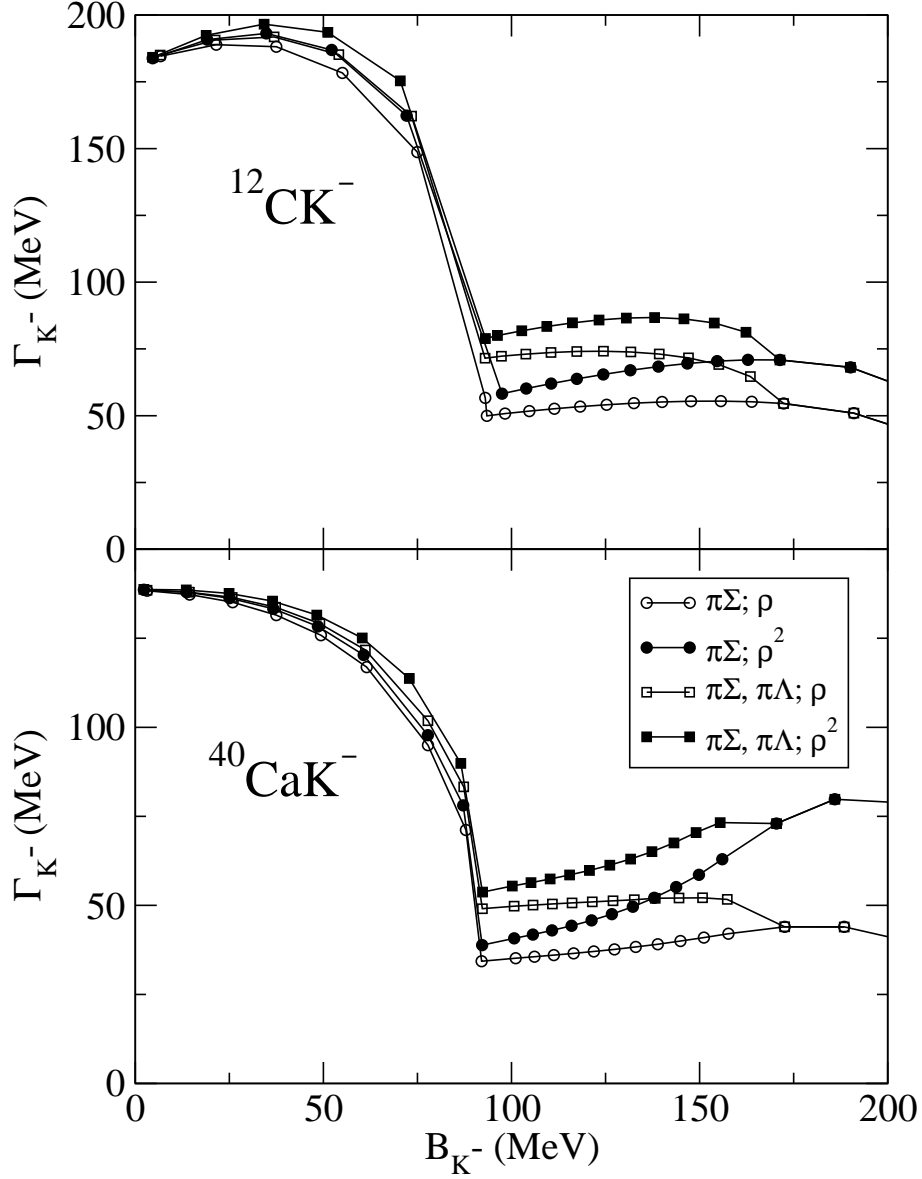


FIG. 2: Widths of the $1s$ K^- -nuclear state in $^{12}_K\text{-C}$ (top panel) and in $^{40}_K\text{-Ca}$ (bottom panel) as a function of the K^- binding energy, for absorption through $\bar{K}N \rightarrow \pi\Sigma$, with and without $\bar{K}N \rightarrow \pi\Lambda$, and assuming ρ or ρ^2 dependence for $\bar{K}NN \rightarrow \Sigma N$ (using the NL-SH RMF model).

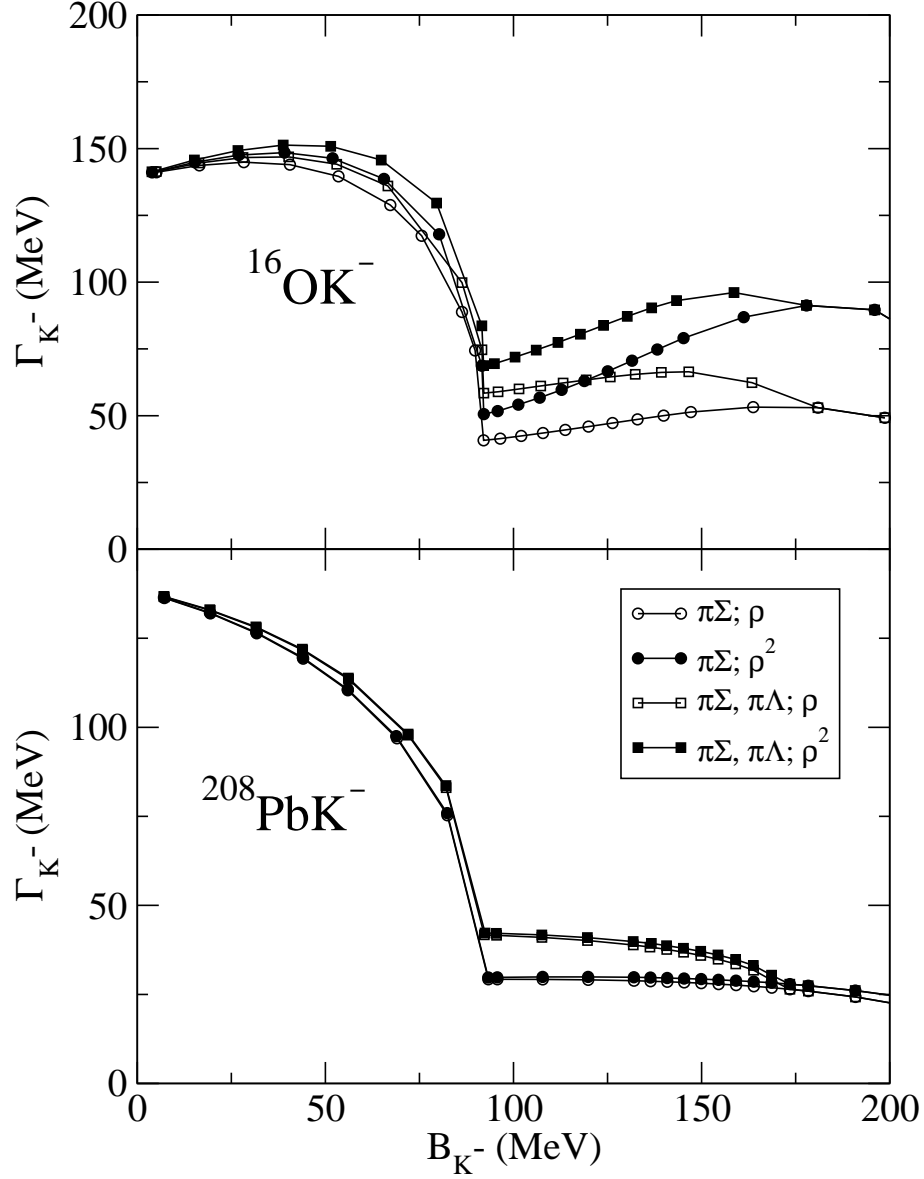


FIG. 3: Widths of the $1s$ K^- -nuclear state in $^{16}_{K^-}\text{O}$ using the NL-SH RMF model (top panel), and in $^{208}_{K^-}\text{Pb}$ using the HS RMF model (bottom panel), as a function of the K^- binding energy for various combinations of and assumptions on the K^- absorption modes as in Fig. 2.

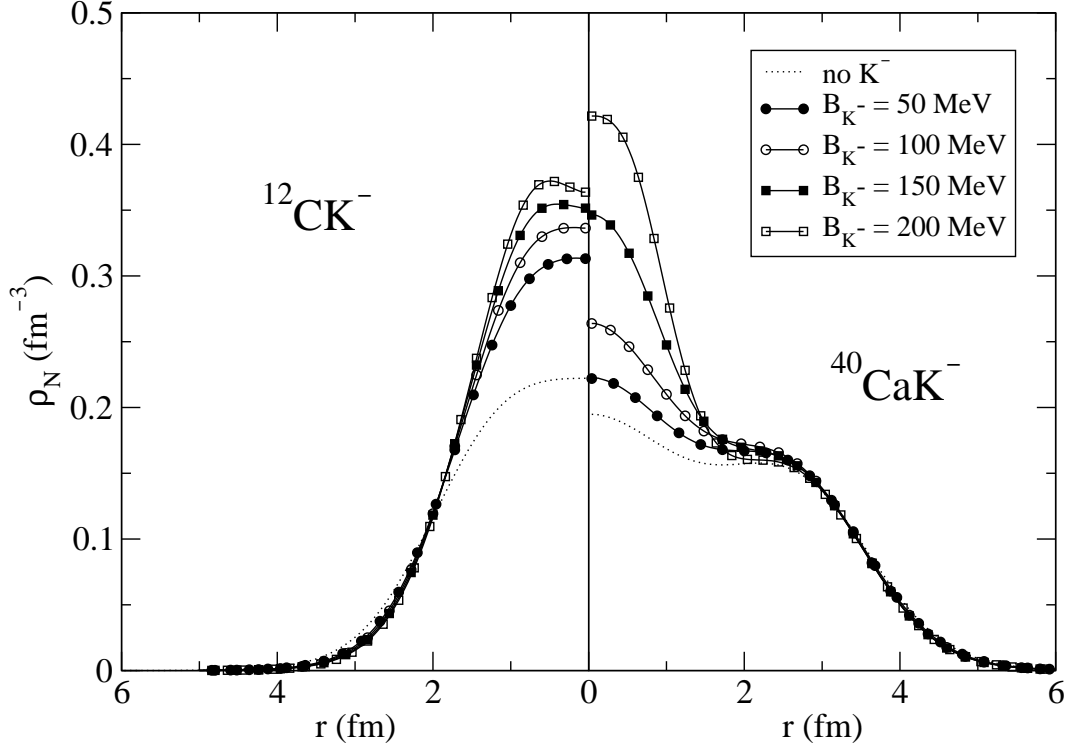


FIG. 4: Nuclear density ρ_N of $^{12}_{K^-}\text{C}$ (left panel) and $^{40}_{K^-}\text{Ca}$ (right panel) for several $1s$ K^- -nuclear states with specified binding energy, using the NL-SH RMF model. The dotted curves denote the corresponding nuclear density in the absence of the K^- meson.

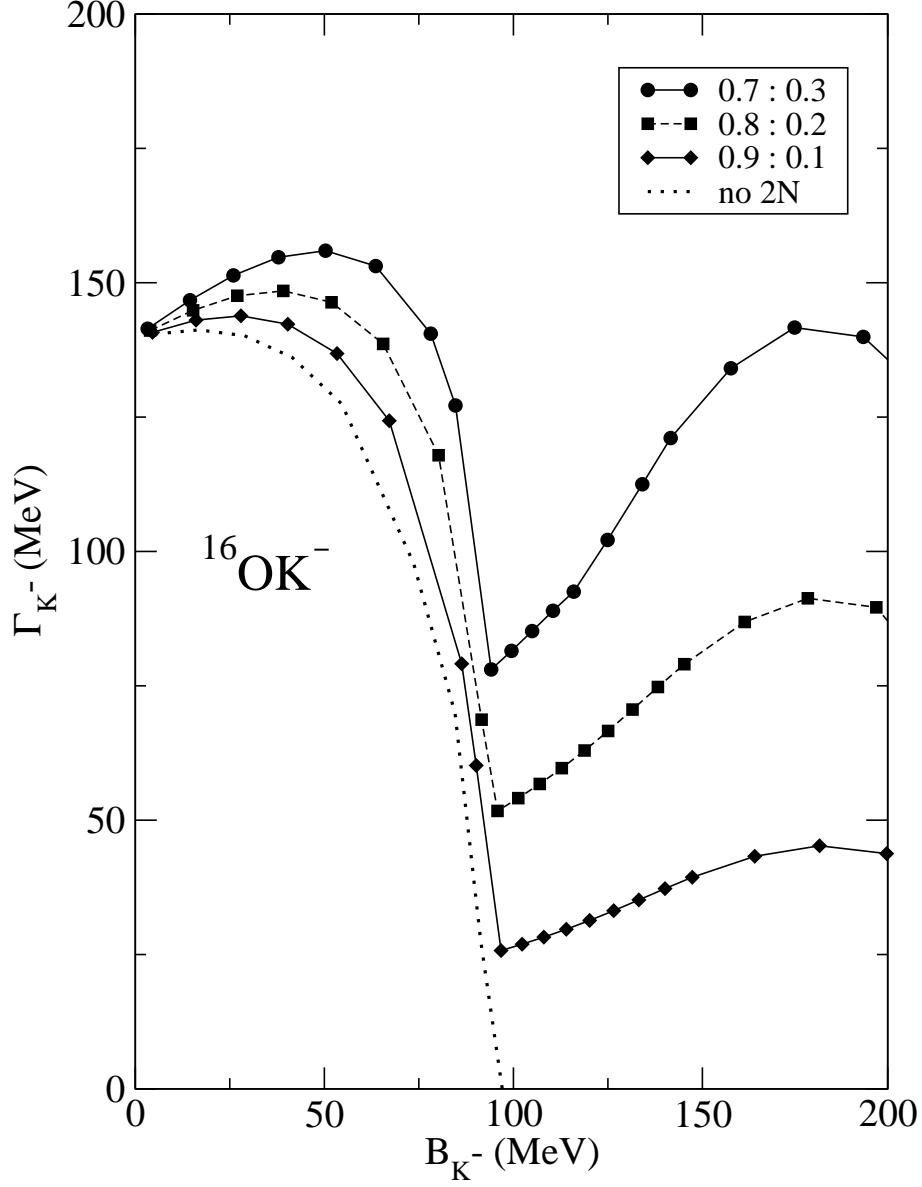


FIG. 5: Widths of the $1s$ K^- -nuclear state in $^{16}_{K^-}\text{O}$ for various absorption branching ratios $\bar{K}N \rightarrow \pi\Sigma : \bar{K}NN \rightarrow \Sigma N$, using the NL-SH RMF model and ρ^2 dependence for the $2N$ -absorption channel. The dotted curve stands for the decay widths in the absence of $2N$ -absorption.

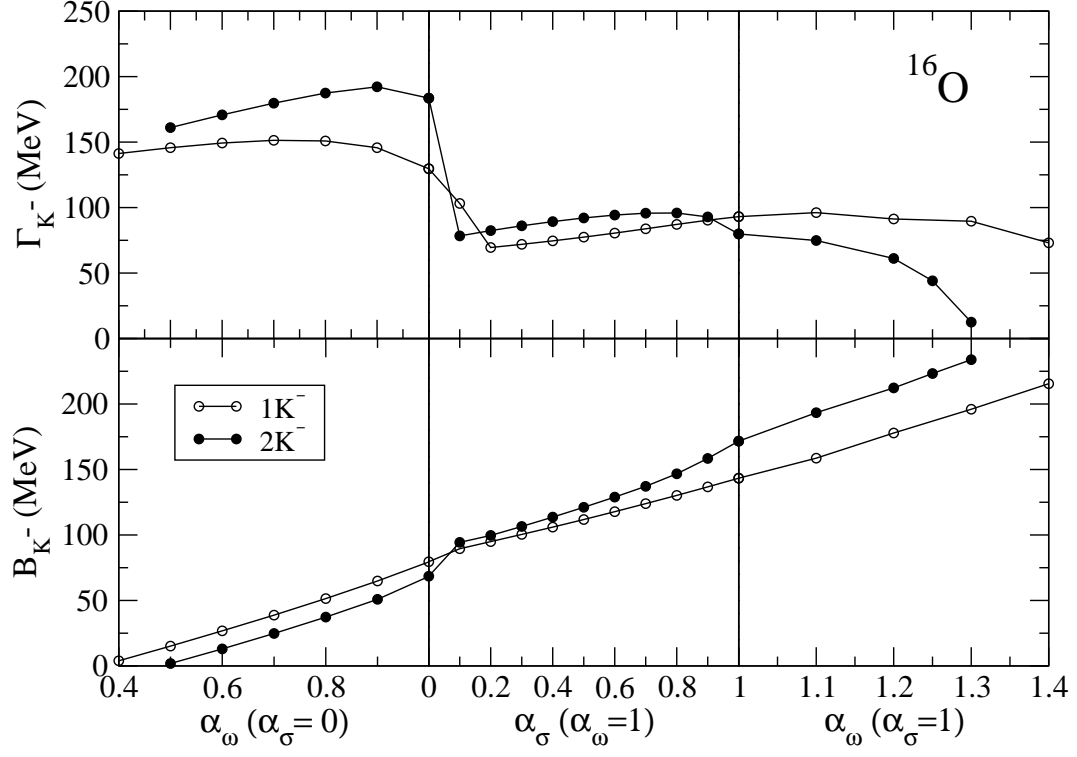


FIG. 6: $1s$ K^- binding energy (bottom panels) and width (top panels) in ^{16}O with one and two antikaon(s) as a function of the coupling strengths α_ω and α_σ (see text), using the NL-SH RMF model.

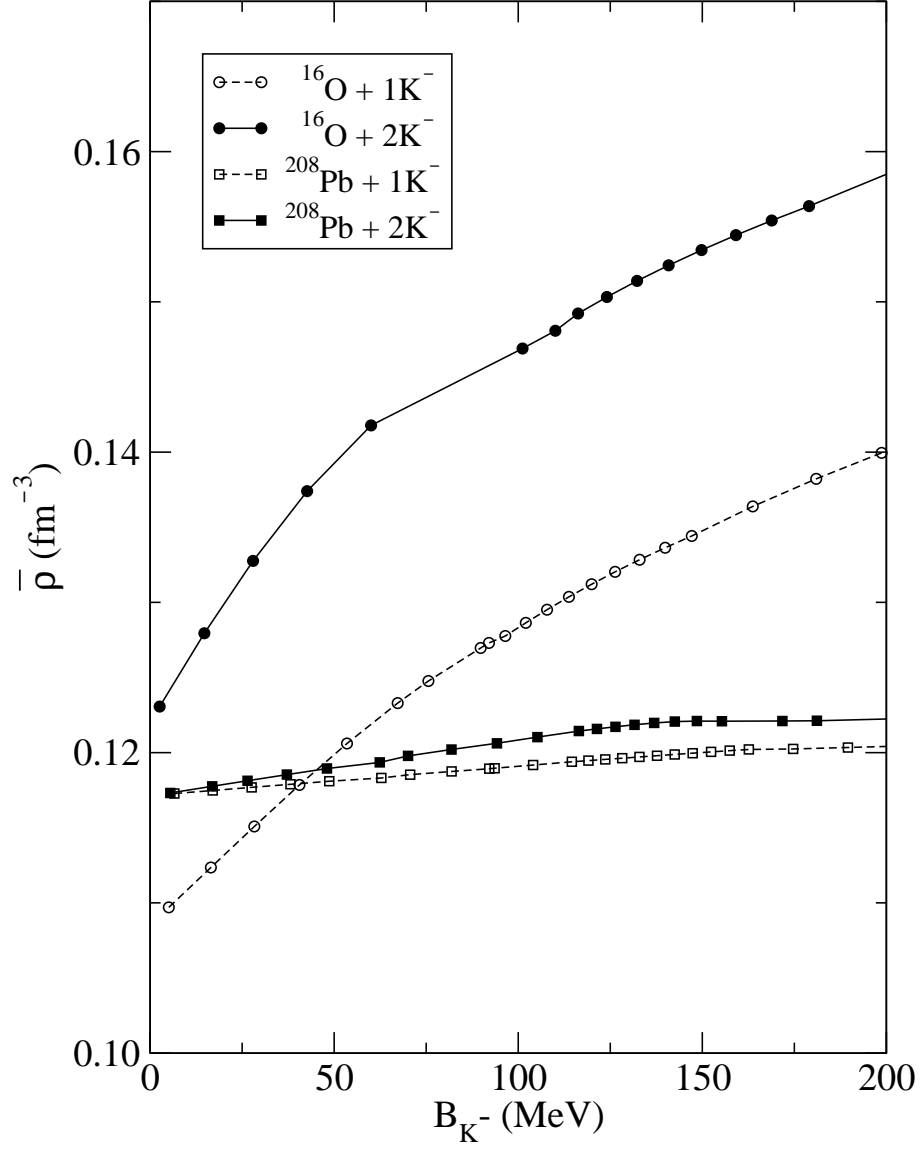


FIG. 7: Average nuclear density $\bar{\rho}$ for ^{16}O and ^{208}Pb with one and two antikaon(s) as a function of the $1s$ K^- binding energy, using the NL-SH RMF model.

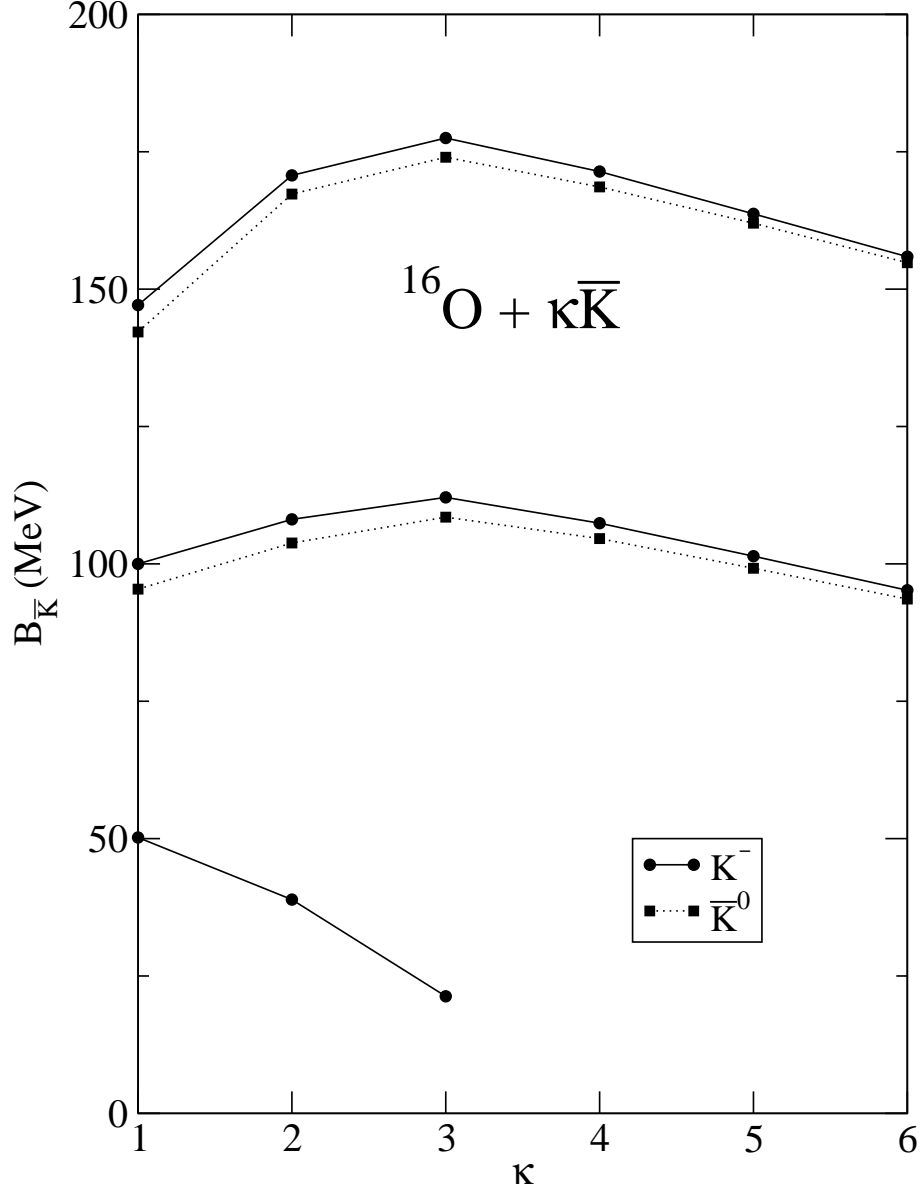


FIG. 8: 1s \bar{K} binding energy $B_{\bar{K}}$ in $^{16}\text{O} + \kappa\bar{K}$, where $\bar{K} = K^-$ (circles) or \bar{K}^0 (squares), as a function of the number κ of antikaons, using the NL-SH RMF model.

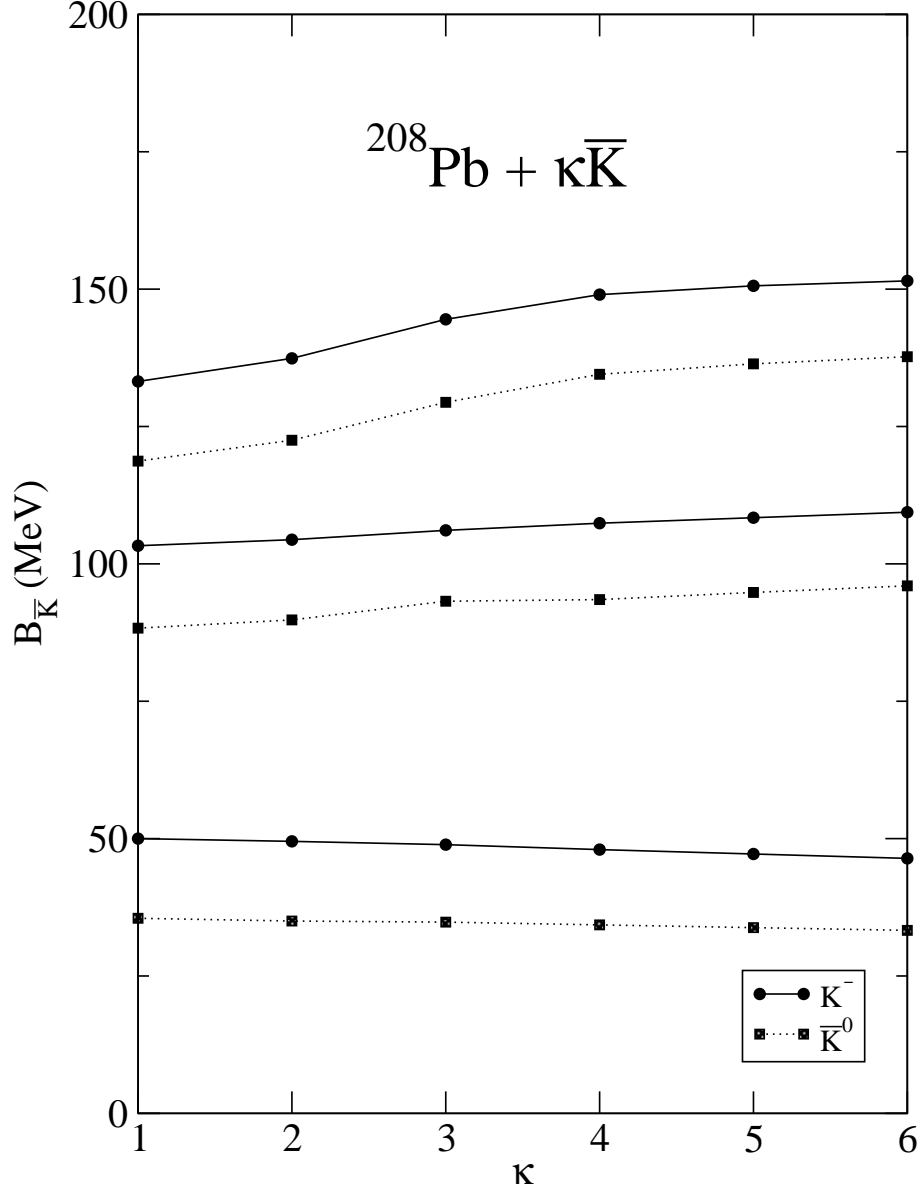


FIG. 9: Same as Fig. 8, but for $^{208}\text{Pb} + \kappa \bar{K}$, where $\bar{K} = K^-$ (circles) and \bar{K}^0 (squares).

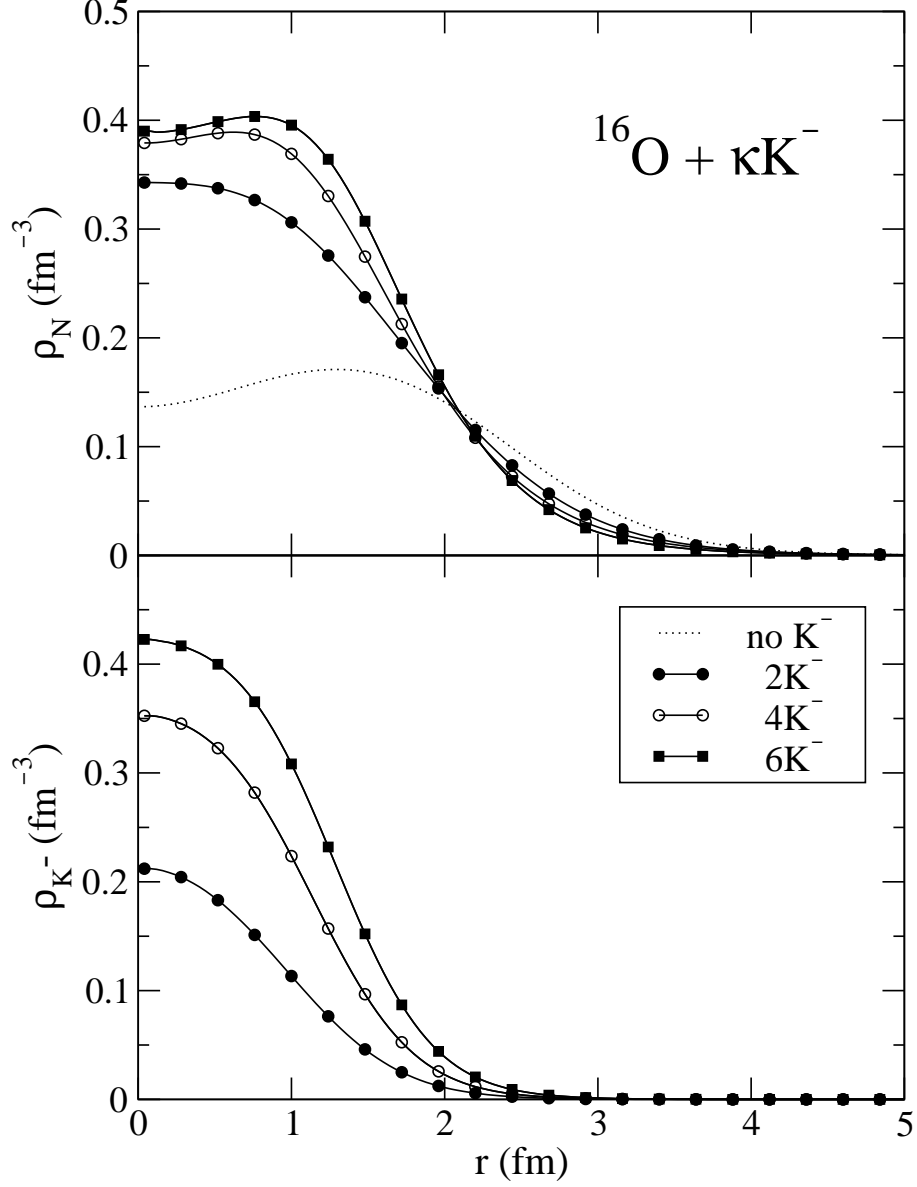


FIG. 10: Nuclear density ρ_N (top panel) and $1s$ K^- density ρ_{K^-} (bottom panel) in $^{16}\text{O} + \kappa K^-$, using the NL-SH RMF model with $\alpha_\sigma = 0.26$ and $\alpha_\omega = 1$, yielding $B_{K^-} = 100$ MeV in $^{16}\text{O} + 1K^-$. The dotted curve stands for the ^{16}O density in the absence of K^- mesons.

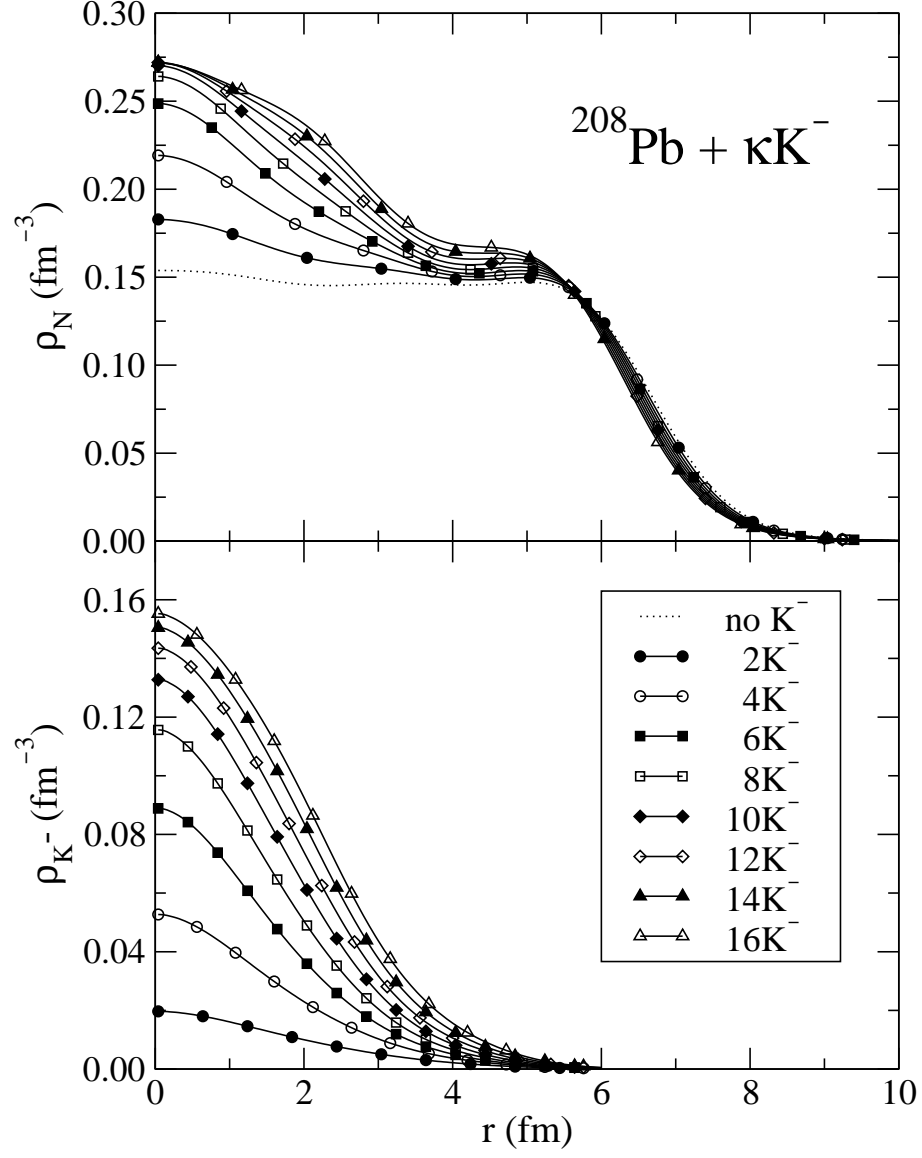


FIG. 11: Same as in Fig. 10, but for $^{208}\text{Pb} + \kappa K^-$ with $\alpha_\sigma = 0$ and $\alpha_\omega = 0.86$, yielding $B_{K^-} = 100$ MeV in $^{208}\text{Pb} + 1K^-$.